HHS Public Access

Author manuscript

Biochemistry. Author manuscript; available in PMC 2024 April 16.

Published in final edited form as:

Biochemistry. 2023 August 01; 62(15): 2252–2256. doi:10.1021/acs.biochem.3c00262.

Dynamic nuclear polarization illuminates key protein-lipid interactions in the native bacterial cell envelope

James E. Kent[1], **Bryce E. Ackermann**[2], **Galia T. Debelouchina**[2,*], **Francesca M. Marassi**[1,3,*]

[1]Sanford Burnham Prebys Medical Discovery Institute, La Jolla CA, 92037, USA

[2]Department Chemistry and Biochemistry, University of California San Diego, La Jolla CA, 92093, USA

[3]Department of Biophysics, Medical College of Wisconsin, Milwaukee WI 53226-3548, USA

Abstract

Elucidating the structure and interactions of proteins in native environments has become a fundamental goal of structural biology. Nuclear magnetic resonance (NMR) spectroscopy is well suited for this task but often suffers from low sensitivity, especially in complex biological settings. Here, we use a sensitivity-enhancement technique called dynamic nuclear polarization (DNP) to overcome this challenge. We apply DNP to capture the membrane interactions of the outer membrane protein Ail, a key component of the host invasion pathway of *Yersinia pestis*. We show that the DNP-enhanced NMR spectra of Ail in native bacterial cell envelopes are well resolved and enriched in correlations that are invisible in conventional solid-state NMR experiments. Furthermore, we demonstrate the ability of DNP to capture elusive interactions between the protein and the surrounding lipopolysaccharide layer. Our results support a model where the extracellular loop arginine residues remodel the membrane environment, a process that is crucial for host invasion and pathogenesis.

Graphical Abstract

*Authors for correspondence

AUTHOR CONTRIBUTIONS. The manuscript was written through contributions of all authors. All authors have given approval to the final version of the manuscript.

ASSOCIATED CONTENT. The Supporting Information provides detailed descriptions of the associated materials and methods.

ACCESSION IDS. Ail: A0A5P8YI02.

The authors declare no competing financial interest.

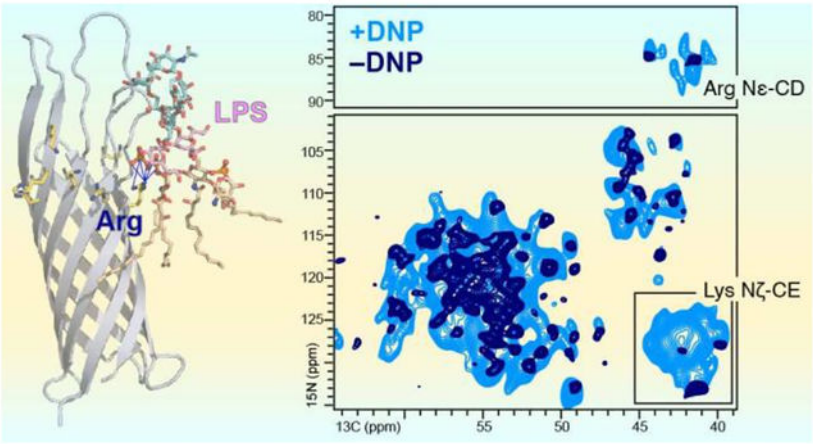

Understanding how proteins interact with their environments at the atomic level is critical for gaining mechanistic biomedical insights. Nuclear magnetic resonance (NMR) is exceptionally well suited for this purpose as NMR signals are highly susceptible to the local environment of their corresponding sites, and therefore, capable of reporting on even very weak intermolecular interactions. Taking advantage of these capabilities, the growing fields of *in situ* and *in cell* NMR[1, 2] present new opportunities for examining protein structure and interactions in native biological contexts, including the investigation of protein aggregation in cellular lysates[3], the characterization of protein function in native membranes[4–6], and the description of protein-drug interactions in cells[2]. Despite these advances, however, a known limitation of NMR is its inherently low signal intensity. The extensive signal averaging times required to accumulate sufficient signal over noise can be impractical for complex samples such as native membranes and cells, and can compromise sample stability. Moreover, signals from sites undergoing chemical or dynamic exchange on the millisecond time scale are difficult to detect. These problems can be particularly limiting for solid-state NMR spectroscopy, which still predominantly relies on the observation of low sensitivity nuclei such as ^{13}C and ^{15}N, and can be sensitive to molecular motions that interfere with the recoupling and decoupling schemes employed in the experiments[7, 8].

The development of high field Dynamic Nuclear Polarization (DNP) for solid-state NMR spectroscopy[9], reviewed in ref.[10–12], provides a key avenue for overcoming these challenges. In a DNP experiment, polarization is transferred from unpaired electron spins to nuclei, typically resulting in enhancements of 10–150 for biological samples. To this end, samples are doped with stable biradicals, and experiments are performed at 90–100 K under magic angle spinning (MAS) conditions. DNP has been used to investigate a wide range of systems, including amyloid fibrils[3, 13], nucleic acids and chromatin polymers[14–16], membrane-embedded proteins[4, 7, 17], and intact cells[18–20]. Here, we use DNP-enhanced solid-state NMR spectroscopy to investigate the lipid interactions of the protein Ail, a virulence factor of the plague pathogen *Yersinia pestis*, in intact bacterial cell envelopes.

Previously, we showed that the *Yersinia pestis* surface protein Ail can be expressed in the outer membrane of *E. coli* cells for *in situ* solid-state NMR structural studies at atomic resolution[5]. The solid-state NMR spectra from isolated bacterial cell envelopes, including

both the inner and outer membranes, and the interleaving peptidoglycan layer, reflect the eight-stranded β-barrel structure of Ail, and reveal sites that interact with bacterial outer membrane components and human serum factors. Moreover, since Ail expression confers some of its key virulence phenotypes to *E. coli*, the structural data from these samples can be correlated with activity. Our previous NMR studies of Ail in bacterial cell envelopes, nanodiscs and liposomes, together with molecular dynamics (MD) simulations and microbiology assays combined with mutagenesis, all suggest that specific interactions between key basic sidechains of Ail with the outer membrane lipopolysaccharide (LPS), that are important for virulence[5, 21]. The data help explain how *Y. pestis* Ail and LPS co-evolved to confer resistance to human innate immunity, and act cooperatively to enhance pathogen survival in serum, antibiotic resistance, and cell envelope integrity[22–25]. Nevertheless, the NMR signals from the LPS binding sites of Ail have been challenging to detect and this limits our understanding of the precise molecular mechanism for this interaction. In this study, we show that the DNP-enhanced solid-state NMR spectra of Ail in bacterial membranes provide direct evidence of contacts between key Arg sidechains of Ail and the outer membrane LPS.

To examine the potential of enhancing the NMR signals from Ail, *in situ*, using DNP, we used a $^{15}N/^{13}C$ labeled Ail sample in intact *E. coli* cell envelopes. The sample was prepared, as previously described[5], by first growing cells in unlabeled media and then transferring them to isotopically labeled media supplemented with both rifampicin and IPTG. Rifampicin halts transcription of the *E. coli* genome and suppresses endogenous protein production, while IPTG induces Ail expression[26]. This protocol of targeted isotopic labeling is critical for suppressing background NMR signals from other cellular components and for yielding high-resolution solid-state NMR spectra of Ail *in situ*[5]. We then doped the sample with 10 mM of the nitroxide-based biradical AMUPol, and cryoprotected the sample in a mixture of 60% glycerol-d_8, 35% D_2O, and 5% H_2O. DNP experiments were performed at 600 MHz and 100 K, with 12 kHz MAS frequency.

Comparison of the one-dimensional spectra obtained with and without electron polarization by microwave irradiation (Fig. 1A–C) demonstrates that DNP yields significant signal enhancement factors ($\varepsilon_{on/off}$) in the range of $\varepsilon_{on/off} = 34$ for ^{1}H-^{15}N cross polarization (CP) to $\varepsilon_{on/off} = 23–31$ for ^{1}H-^{13}C or ^{1}H-^{15}N-^{13}C double CP. DNP signal enhancement is also evident in the two-dimensional $^{13}C/^{13}C$ correlation spectrum (Fig. 1D, E). Although the DNP spectrum exhibits significant line broadening due to the immobilization of ensembles of multiple conformational states at very low temperature (100K), it compares very well with the spectrum obtained at high temperature (278K) without DNP. The overall pattern of cross peaks is conserved, with detectable signals from Ala, Ile, Pro, Ser, Thr and Val spin systems, indicating broadly similar side chain conformations.

Some signals from non-Ail cell envelope components are also enhanced, arising from natural abundance ^{13}C and incorporation of some ^{13}C from the labeled media, and present opportunities to probe specific interactions of Ail with the cell envelope. Previously[5], we showed that several of these signals are visible only in the spectra of Ail(+) cell envelopes, but not Ail(–) cell envelopes, prepared in an identical manner as Ail(+) cell envelopes but from bacteria transformed with empty plasmid lacking the *ail* gene), or Ail(+) liposomes

(Fig. 1E). This suggests that they reflect specific interactions of Ail with the bacterial membrane environment. These resonances could correspond to contacts between His, Lys, Arg and Tyr sidechains of Ail (30–45 ppm) and LPS sugar moieties (60–75 ppm), or alternatively, LPS and lipid contacts resulting from a general ordering effect of Ail on the outer membrane of *E. coli*.

The ^{15}N-filtered two-dimensional ^{15}N/^{13}C correlation NCA spectrum acquired with DNP at 100K also exhibits significant signal enhancement (Fig. 2A). It compares very favorably with its counterpart acquired at 278K, notwithstanding the line broadening, with numerous identifiable signals that could be assigned based on their 278K assignments. Twenty Gly peaks are expected based on the amino acid sequence of Ail (Fig. 2B) and additional signals are observed in the ^{15}N/^{13}CA spectral region associated with Gly (^{13}C: 42–48 ppm; ^{15}N: 101–121 ppm), with one signal (^{13}C: 44.5 ppm; ^{15}N: 121.0 ppm) tentatively assignable to Gly19 in the first extracellular loop of Ail, based on comparison with resonance assignments made in decylphosphocholine micelles[27–29]. These results illustrate the greater amount of information that is available from NMR spectra obtained at low temperature. Moreover, the observation of discrete, resolvable peaks reflects relative order, within narrow conformational ensembles, for their corresponding protein sites rather than high conformational disorder.

Notably, the combined effects of DNP and low temperature also yield a significant enhancement of the signals from Arg sidechains (^{13}C: 40–45 ppm; ^{15}N: 80–90 ppm) which are observable in the NCA spectra due to the similarity of the NE-CD and N-CA spin groups (Fig. 2A). All eight Arg NE-CD signals are visible, in line with the eight Arg residues in the Ail sequence (Fig. 2B). Three Arg are structurally buried in the barrel interior near the intracellular membrane surface (R34, R80 and R155), while the others are located at the extracellular membrane surface (R14, R27, R51, R52, R110) where they can interact with LPS polar groups (Fig. 2C). Here too, the observation of discrete signals at low temperature indicates that their corresponding Arg sites must each adopt a relatively ordered conformational state, since the freezing out of multiple conformations for each site would be expected to result in extensive line broadening and loss of signal intensity. This result also indicates that the AMUPol polarization agent does not induce appreciable paramagnetic broadening in the NMR spectra.

To examine the potential of Ail-LPS contacts as a source of conformational order, we acquired two-dimensional NHHC spectra[30] where through-space contacts between ^{1}H bound to ^{13}C and ^{15}N nuclei are observed as correlations between their respective ^{13}C and ^{15}N nuclei (Fig. 3A). We recorded spectra with DNP, at 100K, for Ail(+) and control Ail(–) cell envelopes.

For Ail(+) compared to Ail(–) cell envelopes, appreciable signal increase is observed for correlations involving amide (^{15}N ~120 ppm) and guanidinium (^{15}N ~70–80 ppm) nitrogens, including Arg sidechains, across the entire ^{13}C spectral region (^{13}C ~15–75 ppm). By contrast, the signal intensity involving amine (^{15}N ~30 ppm) nitrogens, including Lys sidechains, is essentially identical for Ail(+) and Ail(–) samples, with the exception of correlations to CA carbons (54 ppm), which are somewhat more intense in Ail(+). Here, the

abundant amine ^{15}N signal intensity in the Ail(–) cell envelopes may be attributed to amine groups from LPS. The dramatic difference in signal intensity for these regions can also be seen in one dimensional ^{13}C slices extracted from the spectra (Fig. 3B, C).

A closer inspection of the Arg guanidinium spectral region reveals that much of this signal reflects intra-residue contacts (CA ~55 ppm; CB 32 ppm; CG 28 ppm; CD 44 ppm). The ^{13}C signals observed between 62–78 ppm, however, are consistent with the chemical shifts of the peptidoglycan layer, the LPS lipid A moiety (glucosamine, 55–100 ppm; acyl chain, 25–70 ppm) or the LPS core sugars[31]. The unique presence of these correlations in the Ail(+) sample strongly suggests that they reflect interactions between Arg residues on the protein and the outer leaflet LPS. On the other hand, the negligible difference for the characteristic Lys amine NH signals between the Ail(+) and control Ail(–) suggests that interactions between Ail Lys sidechains and LPS are not likely.

This is also consistent with our previous solution NMR and MD simulation data, which suggest key roles for Arg side-chains in establishing specific hydrogen bonds with LPS[21]. Finally, the overall decrease in the amide N signals, which is uniform throughout the entire ^{13}C chemical shift range, is attributed to the effective lack of isotopically labeled protein in the control Ail(–) samples. This is consistent with our previous results[5] showing that Ail(–) bacteria, which are transformed with empty plasmid lacking the *ail* gene, but otherwise grown in an identical manner as Ail(+) bacteria, show no evidence of protein signals when compared with the spectra of Ail(+) preparations.

In summary, we have demonstrated that DNP-enhanced NMR spectroscopy, together with selective labeling strategies, can be used to characterize proteins in their native membrane context with high efficiency and specificity. Despite the line broadening that typically accompanies protein spectra at low temperatures, the spectra of the Ail outer membrane protein are of sufficient quality to allow the identification of many resolved cross peaks and the observation of new peaks that are absent in room temperature spectra. Of note, the new peaks that appear in the Gly and Arg regions of the spectra, for example, display relatively narrow linewidths, indicating that these sites have well defined conformations at low temperature. The sensitivity enhancement afforded by DNP, on the other hand, has allowed us to observe potential interactions between the Ail Arg sidechains and LPS of the outer membrane layer, indicating that these residues can play a fundamental role in the restructuring of the lipid environment around the protein. This was predicted from microbial assays where mutation of key Ail Arg sites resulted in disruption of membrane integrity, suppressed antibiotic resistance and suppressed resistance to human serum, reflecting mutually constructive interactions between Ail and LPS, and highlighting the importance of the Ail–LPS assembly as an organized whole, rather than its individual components[21]. Our results showcase the ability of DNP-enhanced NMR spectroscopy to capture elusive interactions in native samples and to expand the size and complexity of biological systems that can be characterized at atomic resolution. We look forward to future studies that extend these capabilities to Ail in whole cells, and to illuminating its interactions with relevant human host proteins.

Supplementary Material

Refer to Web version on PubMed Central for supplementary material.

ACKNOWLEDGEMENTS.

The authors thank Marassi and Debelouchina lab group members for helpful discussions.

FUNDING SOURCES.

This study was supported by grants from the National Institutes of Health (R35 GM 118186 to F.F.M. and R35 GM138382 to G.T.D.) and the National Science Foundation (NSF MRI CHE 2019066 to G.T.D.).

REFERENCES

(1). Theillet FX (2022) In-Cell Structural Biology by NMR: The Benefits of the Atomic Scale, Chem. Rev 122, 9497–9570. [PubMed: 35357148]

(2). Luchinat E, Cremonini M, and Banci L (2022) Radio Signals from Live Cells: The Coming of Age of In-Cell Solution NMR, Chem. Rev 122, 9267–9306. [PubMed: 35061391]

(3). Frederick KK, Michaelis VK, Corzilius B, Ong TC, Jacavone AC, Griffin RG, and Lindquist S (2015) Sensitivity-enhanced NMR reveals alterations in protein structure by cellular milieus, Cell 163, 620–628. [PubMed: 26456111]

(4). Kaplan M, Narasimhan S, de Heus C, Mance D, van Doorn S, Houben K, Popov-Celeketic D, Damman R, Katrukha EA, Jain P, Geerts WJC, Heck AJR, Folkers GE, Kapitein LC, Lemeer S, van Bergen En Henegouwen PMP, and Baldus M (2016) EGFR Dynamics Change during Activation in Native Membranes as Revealed by NMR, Cell 167, 1241–1251 e1211. [PubMed: 27839865]

(5). Kent JE, Fujimoto LM, Shin K, Singh C, Yao Y, Park SH, Opella SJ, Plano GV, and Marassi FM (2021) Correlating the Structure and Activity of Y. pestis Ail in a Bacterial Cell Envelope, Biophys. J 120, 453–462. [PubMed: 33359463]

(6). Takahashi H, Ayala I, Bardet M, De Paepe G, Simorre JP, and Hediger S (2013) Solid-state NMR on bacterial cells: selective cell wall signal enhancement and resolution improvement using dynamic nuclear polarization, J Am Chem Soc 135, 5105–5110. [PubMed: 23362837]

(7). Bajaj VS, van der Wel PCA, and Griffin RG (2009) Observation of a Low-Temperature, Dynamically Driven Structural Transition in a Polypeptide by Solid-State NMR Spectroscopy, Journal of the American Chemical Society 131, 118–128. [PubMed: 19067520]

(8). Ni QZ, Markhasin E, Can TV, Corzilius B, Tan KO, Barnes AB, Daviso E, Su Y, Herzfeld J, and Griffin RG (2017) Peptide and Protein Dynamics and Low-Temperature/DNP Magic Angle Spinning NMR, J Phys Chem B 121, 4997–5006. [PubMed: 28437077]

(9). Hall DA, Maus DC, Gerfen GJ, Inati SJ, Becerra LR, Dahlquist FW, and Griffin RG (1997) Polarization-enhanced NMR spectroscopy of biomolecules in frozen solution, Science 276, 930–932. [PubMed: 9139651]

(10). Chow WY, De Paëpe G, and Hediger S (2022) Biomolecular and Biological Applications of Solid-State NMR with Dynamic Nuclear Polarization Enhancement, Chem Rev 122, 9795–9847. [PubMed: 35446555]

(11). Biedenbänder T, Aladin V, Saeidpour S, and Corzilius B (2022) Dynamic Nuclear Polarization for Sensitivity Enhancement in Biomolecular Solid-State NMR, Chem Rev 122, 9738–9794. [PubMed: 35099939]

(12). Jaudzems K, Polenova T, Pintacuda G, Oschkinat H, and Lesage A (2019) DNP NMR of biomolecular assemblies, J. Struct. Biol 206, 90–98. [PubMed: 30273657]

(13). Bahri S, Silvers R, Michael B, Jaudzems K, Lalli D, Casano G, Ouari O, Lesage A, Pintacuda G, Linse S, and Griffin RG (2022) (1)H detection and dynamic nuclear polarization-enhanced NMR of Abeta(1–42) fibrils, Proc Natl Acad Sci U S A 119.

(14). Daube D, Vogel M, Suess B, and Corzilius B (2019) Dynamic nuclear polarization on a hybridized hammerhead ribozyme: An explorative study of RNA folding and direct DNP with a paramagnetic metal ion cofactor, Solid State Nucl Magn Reson 101, 21–30. [PubMed: 31078101]

(15). Conroy DW, Xu Y, Shi H, Gonzalez Salguero N, Purusottam RN, Shannon MD, Al-Hashimi HM, and Jaroniec CP (2022) Probing Watson-Crick and Hoogsteen base pairing in duplex DNA using dynamic nuclear polarization solid-state NMR spectroscopy, Proc Natl Acad Sci U S A 119, e2200681119.

(16). Elathram N, Ackermann BE, and Debelouchina GT (2022) DNP-enhanced solid-state NMR spectroscopy of chromatin polymers, J Magn Reson Open 10–11.

(17). Kaplan M, Cukkemane A, van Zundert GC, Narasimhan S, Daniels M, Mance D, Waksman G, Bonvin AM, Fronzes R, Folkers GE, and Baldus M (2015) Probing a cell-embedded megadalton protein complex by DNP-supported solid-state NMR, Nat Methods 12, 649–652. [PubMed: 25984698]

(18). Narasimhan S, Scherpe S, Lucini Paioni A, van der Zwan J, Folkers GE, Ovaa H, and Baldus M (2019) DNP-Supported Solid-State NMR Spectroscopy of Proteins Inside Mammalian Cells, Angew Chem Int Ed Engl 58, 12969–12973. [PubMed: 31233270]

(19). Schlagnitweit J, Friebe Sandoz S, Jaworski A, Guzzetti I, Aussenac F, Carbajo RJ, Chiarparin E, Pell AJ, and Petzold K (2019) Observing an Antisense Drug Complex in Intact Human Cells by in-Cell NMR Spectroscopy, Chembiochem 20, 2474–2478. [PubMed: 31206961]

(20). Ghosh R, Xiao Y, Kragelj J, and Frederick KK (2021) In-Cell Sensitivity-Enhanced NMR of Intact Viable Mammalian Cells, Journal of the American Chemical Society 143, 18454–18466. [PubMed: 34724614]

(21). Singh C, Lee H, Tian Y, Schesser Bartra S, Hower S, Fujimoto LM, Yao Y, Ivanov SA, Shaikhutdinova RZ, Anisimov AP, Plano GV, Im W, and Marassi FM (2020) Mutually constructive roles of Ail and LPS in Yersinia pestis serum survival, Mol. Microbiol 114, 510–520. [PubMed: 32462782]

(22). Parkhill J, Wren BW, Thomson NR, Titball RW, Holden MT, Prentice MB, Sebaihia M, James KD, Churcher C, Mungall KL, Baker S, Basham D, Bentley SD, Brooks K, Cerdeno-Tarraga AM, Chillingworth T, Cronin A, Davies RM, Davis P, Dougan G, Feltwell T, Hamlin N, Holroyd S, Jagels K, Karlyshev AV, Leather S, Moule S, Oyston PC, Quail M, Rutherford K, Simmonds M, Skelton J, Stevens K, Whitehead S, and Barrell BG (2001) Genome sequence of Yersinia pestis, the causative agent of plague, Nature 413, 523–527. [PubMed: 11586360]

(23). Deng W, Burland V, Plunkett G 3rd, Boutin A, Mayhew GF, Liss P, Perna NT, Rose DJ, Mau B, Zhou S, Schwartz DC, Fetherston JD, Lindler LE, Brubaker RR, Plano GV, Straley SC, McDonough KA, Nilles ML, Matson JS, Blattner FR, and Perry RD (2002) Genome sequence of Yersinia pestis KIM, J Bacteriol 184, 4601–4611. [PubMed: 12142430]

(24). Knirel YA, and Anisimov AP (2012) Lipopolysaccharide of Yersinia pestis, the Cause of Plague: Structure, Genetics, Biological Properties, Acta Naturae 4, 46–58. [PubMed: 23150803]

(25). Kolodziejek AM, Hovde CJ, and Minnich SA (2012) Yersinia pestis Ail: multiple roles of a single protein, Front Cell Infect Microbiol 2, 103. [PubMed: 22919692]

(26). Almeida FC, Amorim GC, Moreau VH, Sousa VO, Creazola AT, Americo TA, Pais AP, Leite A, Netto LE, Giordano RJ, and Valente AP (2001) Selectively labeling the heterologous protein in Escherichia coli for NMR studies: a strategy to speed up NMR spectroscopy, J Magn Reson 148, 142–146. [PubMed: 11133287]

(27). Ding Y, Fujimoto LM, Yao Y, Plano GV, and Marassi FM (2015) Influence of the lipid membrane environment on structure and activity of the outer membrane protein Ail from Yersinia pestis, Biochim Biophys Acta 1848, 712–720. [PubMed: 25433311]

(28). Marassi FM, Ding Y, Schwieters CD, Tian Y, and Yao Y (2015) Backbone structure of Yersinia pestis Ail determined in micelles by NMR-restrained simulated annealing with implicit membrane solvation, J. Biomol. NMR 63, 59–65. [PubMed: 26143069]

(29). Dutta SK, Yao Y, and Marassi FM (2017) Structural Insights into the Yersinia pestis Outer Membrane Protein Ail in Lipid Bilayers, J Phys Chem B 121, 7561–7570. [PubMed: 28726410]

(30). Lange A, Luca S, and Baldus M (2002) Structural constraints from proton-mediated rare-spin correlation spectroscopy in rotating solids, J. Am. Chem. Soc 124, 9704–9705. [PubMed: 12175218]

(31). Laguri C, Silipo A, Martorana AM, Schanda P, Marchetti R, Polissi A, Molinaro A, and Simorre JP (2018) Solid State NMR Studies of Intact Lipopolysaccharide Endotoxin, ACS Chem Biol 13, 2106–2113. [PubMed: 29965728]

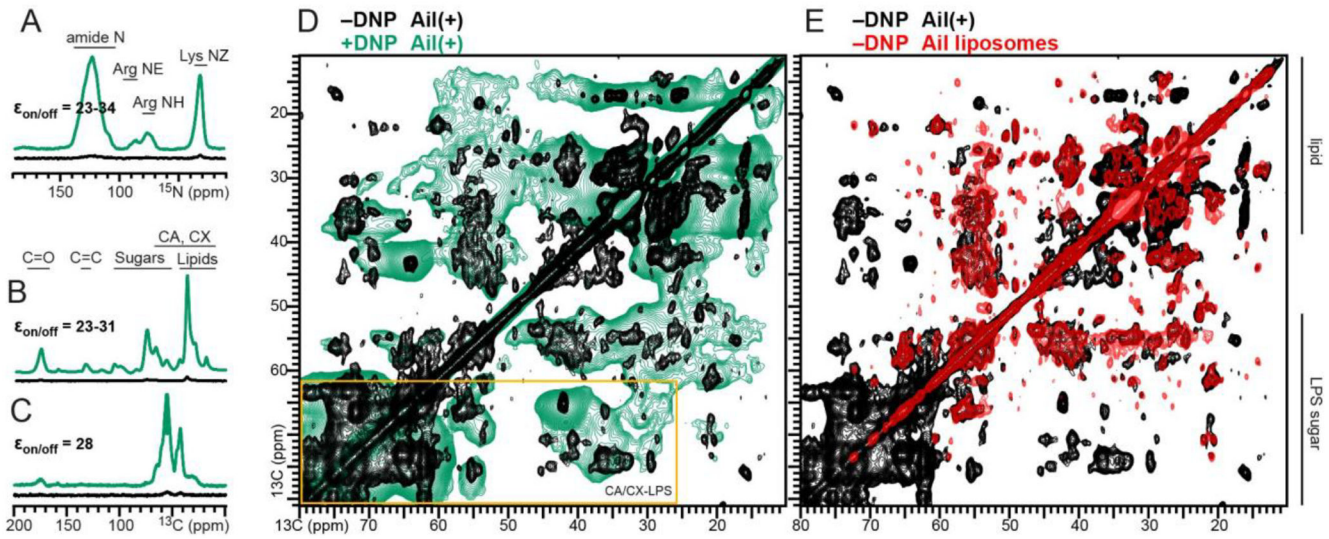

Figure 1. DNP signal enhancement of the ^{15}N and ^{13}C MAS solid-state NMR spectra of Ail in *E. coli* cell envelopes.

(A-C) One dimensional spectra acquired with (A) ^{1}H-^{15}N CP, (B) ^{1}H-^{13}C CP, or (C) ^{1}H-^{15}N-^{13}C double CP, and with (green) or without (black) microwave irradiation. Signal enhancement factors ($\varepsilon_{on/off}$) were measured as the ratio of signal intensity observed with and without microwave irradiation. **(D, E)** Two dimensional ^{13}C/^{13}C correlation spectrum of Ail in *E. coli* cell envelopes acquired with DNP (green). The spectra from Ail in *E. coli* cell envelopes (black) and Ail in liposomes (red), acquired without DNP are shown for comparison and were described previously[5]. The yellow rectangle marks LPS-related correlations.

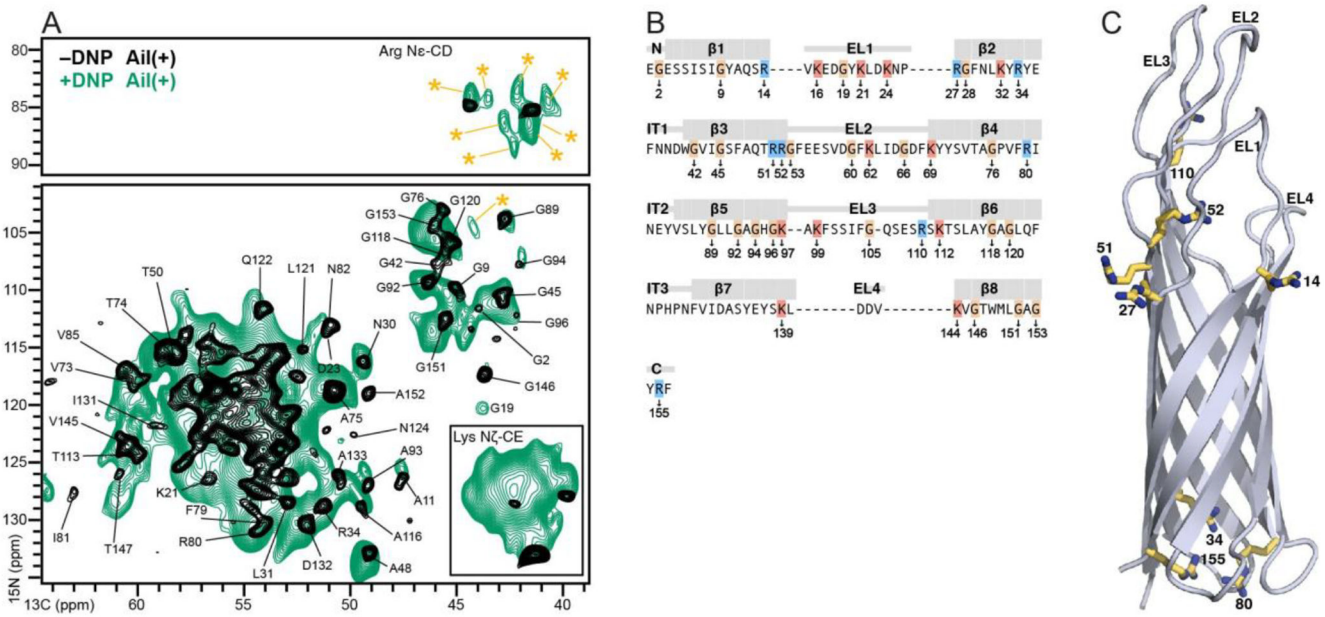

Figure 2. Two-dimensional NCA spectrum of $^{15}N,^{13}C$-Ail in *E. coli* cell envelopes acquired with DNP (green).

(A) Resolved assigned peaks are marked. Asterisks denote a new unassigned peak observed with DNP. The spectrum from Ail in *E. coli* cell envelopes (black) acquired without DNP is shown for comparison and was described previously[5]. **(B)** Amino acid sequence of Ail. The eight β-strands (β1-β8), four extracellular loops (EL1-EL4) and three intracellular turns (IT1-IT3) are mapped above the sequence. There are 8 Arg (blue), 11 Lys (red), and 20 Gly residues. **(C)** Snapshot of the Ail β-barrel obtained after 1.5 μs of MD simulation in a *Y. pestis* outer membrane depicting the eight Arg residues.

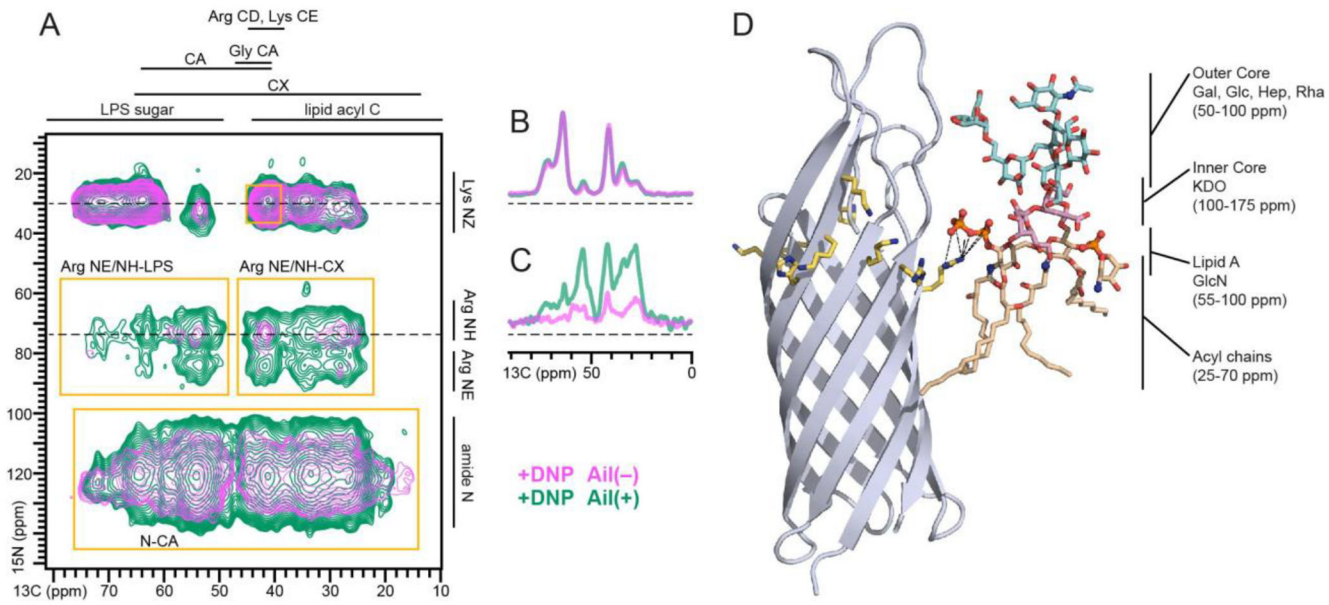

Figure 3. Two-dimensional NHHC spectra acquired with DNP.

(A-C) Spectra were acquired for (15N,13C)-Ail(+) (green) or (^{15}N,^{13}C)-Ail(–) (pink) *E. coli* cell envelopes. Spectral regions of correlations are marked (gold boxes). One-dimensional slices (B, C) were taken at specific ^{15}N chemical shifts (dashed lines) of sidechain N from Arg and Lys. **(D)** Snapshot of Ail obtained after 1.5 μs of MD simulation in a *Y. pestis* outer membrane showing that Arg27 in the LPS-recognition motif establishes multiple interactions with lipid A of an LPS molecule. Characteristic ^{13}C chemical shifts of the different LPS groups are marked. MD simulations were described previously[21].